# Molecular Mobility of Peroxy Radicals at the Ends of Nonisolated Polystyrene Chains Tethered on the Solid Surface of Poly(tetrafluoroethylene) in a Vacuum

**Masato Sakaguchi,*,† Takeru Iwamura,† Katsuhiro Yamamoto,‡ Yohei Miwa,‡ Shigetaka Shimada,‡ and Masahiro Sakai§**

*Institute for Environmental Sciences, University of Shizuoka, 52-1, Yada, Suruga-ku, Shizuoka 422-8526, Japan, Department of Materials Science & Engineering, Nagoya Institute of Technology, Gokiso-cho, Showa-ku, Nagoya 466-8555, Japan, and Research Center for Molecular-Scale Nanoscience, Institute for Molecular Science, 38, Nishigo-Naka, Myodaiji, Okazaki 4444-8585, Japan*

*Received August 27, 2007; Revised Manuscript Received November 8, 2007*

ABSTRACT: The molecular mobility of peroxy radicals at the ends of nonisolated polystyrene chains (NIPSOO) tethered on the solid surface of poly(tetrafluoroethylene) (PTFE) in a vacuum was investigated in the temperature range from 10 to 250 K by electron spin resonance spectroscopy (ESR). The train−tail transition temperature of the NIPSOO tethered on the solid surface of PTFE in a vacuum was estimated to be 200 K, which was 40 K higher than that of the peroxy radicals at the ends of the isolated polystyrene chains (IPSOO) (Sakaguchi, M.; Yamamoto, K.; Miwa, Y.; Shimada, S.; Sakai, M.; Iwamura, T. *Macromolecules* **2007**, *40*, 1708; ref 1) tethered on the solid surface of PTFE in a vacuum. The activation energy (12.2−14.9 kJ/mol) of the NIPSOO of the tail state was large value compared to that (8.3−9.2 kJ/mol) (Sakaguchi, M.; Yamamoto, K.; Miwa, Y.; Shimada, S.; Sakai, M.; Iwamura, T. *Macromolecules* **2007**, *40*, 1708; ref 1) of IPSOO of the tail state. The high transition temperature and the large activation energy of the NIPSOO compared to those of the IPSOO are probably due to nonisolated chains, which take place in contacts and pseudo entanglements with inter- and neighboring-polystyrene chains on the PTFE surface.

## Introduction

Many kinds of polymers are widely used in industry and in our life. Many research studies have been reported on the mobility of polymer chains in the bulk. They indicate that the mobility of the polymer chain relates to the amount and size of the free volume in the bulk. On the other hand, a surface of solid polymer plays an important part in painting, coating, friction, wetting or adhesion, and so on. Recently, some research groups focused on the mobility of chains on the surface of solid polymers. The motion of chains located near the surface was enhanced compared to that in the bulk polymer.[2] A glass transition temperature ($T_g$) for freely standing films was reduced below the bulk value and decreased with film thickness.[3−5] The reduction of $T_g$ in freely standing polymer thin films was due to the decrease of the cooperative length scale for chain segments near the surface.[6] The mobility of chains increased toward the free surfaces due to the decrease in the density of thin polyethylene films.[7] A glass transition temperature at the surface ($T_g^s$) of the polystyrene film was lower than that in the bulk ($T_g^b$).[8−12] The reduction of the $T_g^s$ of the polystyrene film surface was attributed to the excess free volume generated by the chain ends at the surface. The excess free volume led to a decrease in the chain segmental density at the surface and promoted chain activity.[9,11,12] The reduction in the local $T_g$ on approaching the surface of polystyrene was observed by using low-energy muons, which were used to probe the local motion in a thin film of polystyrene as a function of depth below the free surface.[13]

Many researchers have been focused on the chain activity at the surface of a thin film which has low segmental density compared to the bulk. On the contrary, we have studied the mobility of polymer chains tethered on the solid surface of poly(tetrafluoroethylene) (PTFE), which have extremely low chain segmental density on the surface.[14−23] We have reported that the mobility of any polymer chain tethered on the surface was higher than that in the bulk. It can be said that the "isolated polymer chains" tethered on the solid surface of PTFE have an ultimately low chain segmental density. The isolated polymer chain can be expected to show extremely active motion. In our previous article,[1] the motional correlation time and activation energy of the peroxy radicals at the ends of the isolated polystyrene chains (IPSOO) tethered on the solid surface of PTFE in a vacuum were evaluated by spectral simulations and the train−tail transition temperature and the activation energy at the tail state were estimated as 160 K and 8.3−9.2 kJ/mol.

Here we report the mobility of peroxy radicals at the ends of nonisolated polystyrene chains (NIPSOO) tethered on the solid surface of PTFE, in which the chain segmental density is probably higher than that of the IPSOO due to interaction between inter- and neighboring chains.

## Experimental Section

The inhibitor in the styrene monomer (St, Cica pure reagent, Kanto Chemical Co., Ltd) was adsorbed to activated aluminum oxide (particle size 2−4 mm, Kanto Chemical Co., Ltd). Oxygen gas dissolved in St was eliminated by four repeated times of the freeze−pump−thaw method in a vacuum line. The St was purified by distilling twice in the vacuum line. PTFE (Fluon G163, Asahi Glass Co., Ltd) was used without further purification.

The polystyrene (PS) chains tethered on the solid surface of PTFE in a vacuum were produced by the same procedure as descried in our previous paper[1] except for the amount of St monomer. The

* Corresponding author. Masato Sakaguchi. E-mail: sakaguchi@u-shizuoka-ken.ac.jp. Phone +81-54-264-5786, fax +81-54-264-5786.
† University of Shizuoka.
‡ Nagoya Institute of Technology.
§ Institute for Molecular Science.

10.1021/ma701925v CCC: $40.75 
Published on Web 12/06/2007

following procedure was used: The solid PTFE (1.5 g) in a glass-ball-mill connected to a vacuum line was evacuated under 0.6 Pa pressure at 353 K for 4 h. The purified St ($1.7 \times 10^{-3}$ mol) was introduced into the glass-ball-mill in the vacuum line. The glass-ball-mill containing solid PTFE and St was sealed off from the vacuum line and set in a vessel filled with liquid nitrogen. The solid sample of PTFE and St in the glass-ball-mill was mechanically fractured by a homemade vibration ball-mill apparatus for 21 h at 77 K in a vacuum.[1,24] After milling, the powdered sample was dropped into an ESR sample tube attached to the top of the glass-ball-mill.

ESR spectra were observed at a microwave power level of 0.1 mW to avoid power saturation and with 100 kHz field modulation using a Bruker ESP300E spectrometer (X-band) equipped with a helium cryostat (Oxford ESR 900) and a temperature controller (Oxford ITC4). Before ESR observation, the sample was cooled to 4 K in the cryostat and held for 1 h. The sample was kept at elevated temperature for 15 min, then ESR spectra were observed at the temperature.

ESR spectral simulation was carried out by using a computer program which can calculate a line shape equation of ESR spectra in the solid-state having anisotropic **g** and hyperfine splitting tensors **A** as has been shown in the previous paper.[1] The computer program was made based on the concept as follows: The complex magnetization, *Z*, is given by

$$Z = -iC\mathbf{S}^{-}\sum_{j=1}^{n_L} D_j \mathbf{M}_{0j}^{-1}\mathbf{P} \qquad (1)$$

According to Heinzer's definition,[25] $\mathbf{M}_0$ is a complex non-Hermitian matrix of dimension $N = n_C n_L$, with $n_C$ = number of chemical configurations and $n_L$ = number of lines. **P** is a population. $\mathbf{S}^-$ is shift operator. The degeneracy of a transition is denoted by $D_j$. The *C* denotes a scaling factor. The imaginary part of *Z* yields the absorption line shape equation directly. $\mathbf{M}_{0j}$ can be decomposed into a constant matrix, **F**, and a scalar matrix, $iH\mathbf{E}$, which are exhibited with a magnetic field unit instead of a frequency unit:

$$\mathbf{M}_{0j} = \mathbf{F}_j + iH\mathbf{E}$$

with

$$\mathbf{F}_j = \sum_{r=1}^{nc}\sum_{s=1}^{nc}[-i\,\delta_{rs}(H_r^0 + \sum_{\alpha=1}^{nA} A_{r\alpha}) - \delta_{rs}(1/T_2) - \delta_{rs}\sum_{n\neq r}^{nc} K_{rn} + (1-\delta_{rs})K_{sr}]$$

$$K_{sr} = (1/\tau_r)(h/2\pi)\omega_{0,r}/(g_r\beta)$$

$$1/T_2 = (1/T_{2,r})(h/2\pi)\omega_r/(g_r\beta)$$

$$H_r^0 = (h/2\pi)\omega_r/(g_r\,\beta)$$

$$g_r^{\,2} = g_{r1}^{\,2}\cos^2\phi\sin^2\theta + g_{r2}^{\,2}\sin^2\phi\sin^2\theta + g_{r3}^{\,2}\cos^2\theta$$

$$A_r^{\,2} = A_{r1}^{\,2}\cos^2\phi\sin^2\theta + A_{r2}^{\,2}\sin^2\phi\sin^2\theta + A_{r3}^{\,2}\cos^2\theta$$

$K_{sr}$ is treated as the rate of conformation change from *r* to *s*. $\tau_r$ is a correlation time denoted by a residence time of the *r* conformation. $H_r^0$ is an electronic Zeeman interaction of the *r* conformation. $1/T_2$ is a line width. The $g_r$ and $A_r$ are *g* values and the hyperfine splitting constant at the *r* conformation. The last two terms, $-\delta_{rs}\sum_{n\neq r}^{n_c} K_{rn} + (1-\delta_{rs})K_{sr}$, are responsible for the intramolecular exchange.

The coordinate system of a peroxy radical revealing the principal direction of the **g** tensor is shown in Figure 1. Site 1 is defined as the direction of the $g_1$ (2.0355) axis (that is, the direction of the maximum principal value)[26,27] which is parallel to the axis of the oxygen−oxygen bond, the direction of the $g_3$ (2.0023) axis (that is, the direction of the minimum principal value)[26,27] parallel to the direction of the *p* orbital and perpendicular to the C−O−O plane, and the $g_2$ (2.0080) axis that is perpendicular to both the $g_1$ and $g_3$ axes. Two other sites were defined as follows: Site 2 (2.0080, 2.0355, 2.0023) and Site 3 (2.0355, 2.0023, 2.0080). In our spectral simulation, we assumed that a peroxy radical stayed at site *r* with a correlation time $\tau_r$ and then jumped to another site. The correlation time without distribution was assumed. The Gaussian distribution function was employed as a line shape function.

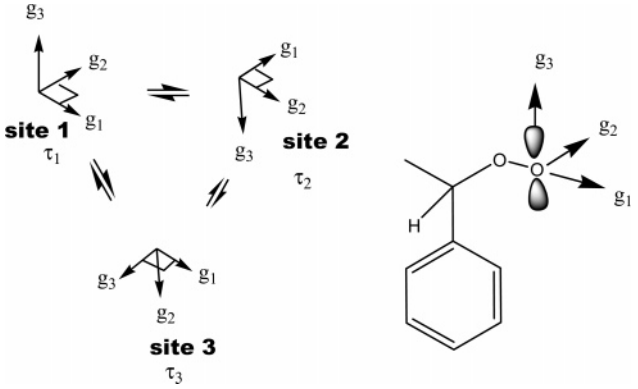


**Figure 1.** Coordinate system of the peroxy radical showing principal direction of the **g** tensor ($g_1 = 2.0355 \pm 0.00005$, $g_2 = 2.0080 \pm 0.00005$, and $g_3 = 2.0023 \pm 0.00005$). Site 1 is defined as the direction of the $g_1$ (2.0355) axis and is parallel to the axis of the oxygen−oxygen bond, the direction of the $g_3$ (2.0023) axis is parallel to the direction of the *p* orbital and perpendicular to the C−O−O plane, and the $g_2$ (2.0080) axis is perpendicular to both the $g_1$ and $g_3$ axes. Sites 2 and 3 are defined as (2.0080, 2.0355, 2.0023) and (2.0355, 2.0023, 2.0080).

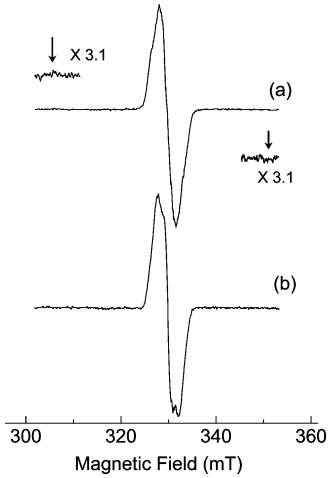


**Figure 2.** ESR spectra observed at 77 K: (a) as-fractured PTFE with St monomer in a vacuum at 77 K; (b) annealing at 213 K for 10 min. Arrows indicate that there are no wing peaks due to the PTFE mechano radicals, $-CF_2CF_2^{\bullet}$.

## Results and Discussion

Figure 2a shows the ESR spectrum observed at 77 K of PTFE milled with St in a vacuum at 77 K. The arrows indicate that there are no wing peaks due to the PTFE mechano radicals: $-CF_2CF_2^{\bullet}$, which are produced by mechanical fracture of PTFE.[1,24] The disappearance of the wing peaks is due to a reaction of PTFE mechano radicals with St monomer and PTFE mechano radicals resulting in PS propagating radicals. To complete the reaction, the sample was annealed at 213 K for 10 min (Figure 2b). We reported that mechano radicals were localized on the fresh surface of fractured polymers.[28,29] The PTFE mechano radicals initiated a radical polymerization of several monomers, such as ethylene,[15,23] methymethacrylate,[30]

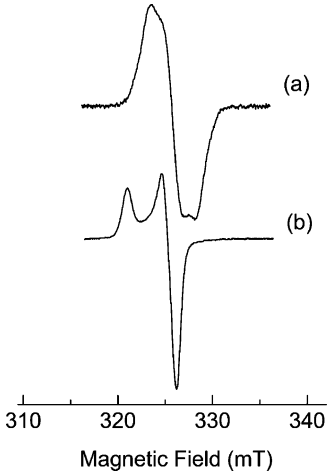


**Figure 3.** Spectral change with advancing of the oxidation reaction from the chain end-type alkyl radicals of PS at the ends of NIPS to the peroxy radicals: (a) after contact with oxygen molecules at 77 K; (b) after annealed at 171 K for 10 min. All spectra were observed at 77 K.

isobutylene,[31] and 1,3-butadiene.[32] It was found that the mechanical fracture of PTFE (1.5 g) with St ($1.2 \times 10^{-5}$ mol) in a vacuum at 77 K produced PTFE mechano radicals.[1] The PTFE mechano radicals initiated a radical polymerization of St and produced isolated polystyrene chains tethered on the solid surface of PTFE. The *g*-values of the observed peroxy radical of the PS were smaller than those of PTFE.[16] Taking into account the past result, the singlet spectrum of Figure 2b can be assigned to PS propagating radicals.

Assuming no residue of St, the average degree of polymerization (DP) of PS can be estimated as DP $\leq 1.0 \times 10^4$ from the concentrations of St ($1.7 \times 10^{-3}$ mol) and PTFE mechano radicals ($6.8 \times 10^{16}$ radicals/g) located on the surface of PTFE.[15] The radius of gyration ($R_g = (C_\infty(2\mathrm{DP} - 1)a_b^2/6)^{0.5}$) of PS was calculated to be 28 nm on the basis of the $1.0 \times 10^4$ of DP, carbon−carbon bond length ($a_b = 0.15351$ nm)[33] and characteristic ratio ($C_\infty = 10.46$) of atactic PS.[34] The area per tethered point on the PTFE surface was calculated to be 31 nm$^2$ on the basis of the concentration of PTFE mechano radicals located on the surface and specific surface area (2.1 m$^2$/g).[15] Assuming the area of a circle as 31 nm$^2$, the radius per tethered point ($R_t$) is 3.1 nm. The relative radius ($R_L = R_g/R_t$) of PS having $1.0 \times 10^4$ of DP is to be 8.9, which is one order higher than 0.77 of isolated PS chains tethered on the PTFE surface.[1] Since the tethered PS chain having $R_L = 8.9$ is larger than 1.0, it can contact and entangle with inter- and neighboring-PS chains on the PTFE surface. The entanglement can be regarded as a "pseudo entanglement" which can be untangled at elevated temperatures. Thus, the PS chain tethered on the PTFE surface can be regarded as a "nonisolated PS chain" (NIPS). The NIPS chain has a free radical at the terminal of the chain because the terminal of the NIPS chain is a PS propagating radical (Figure 2b).

The NIPS chains were in contact with oxygen molecules at 77 K (Figure 3a). After annealing at 171 K for 10 min, the ESR spectrum observed at 77 K was drastically changed and showed a characteristic powder pattern of peroxy radicals, in which a molecular motion of the peroxy radicals was in a rigid limit (Figure 3b). Hereafter the ends of the peroxy radicals of the NIPS chains tethered on the solid surface of PTFE are called "peroxy radicals at the ends of the nonisolated PS chains" (NIPSOO). The NIPSOO is located on the PTFE surface and may have a bulky shape induced from high chain segmental density (illustrated in Figure 4, train state).

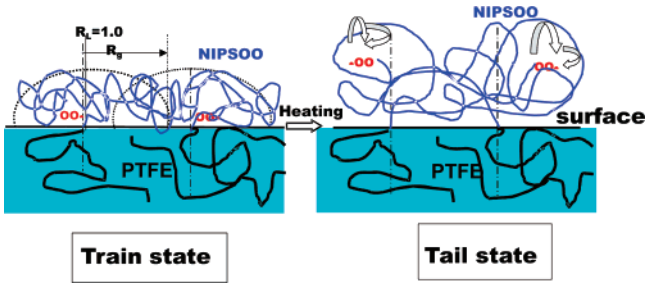


**Figure 4.** Schematic illustration of NIPSOO tethered on the PTFE surface in a vacuum, which take a train state below 190 K and a tail state above 200 K. $R_g$, radius of gyration; $R_L = R_g/R_t$, a relative radius to a radius of a tethered point, $R_t$. $R_L = 1.0$, a critical length for the PS chain in which it can contact and entangle with inter- and neighboring-PS chains on the PTFE surface.

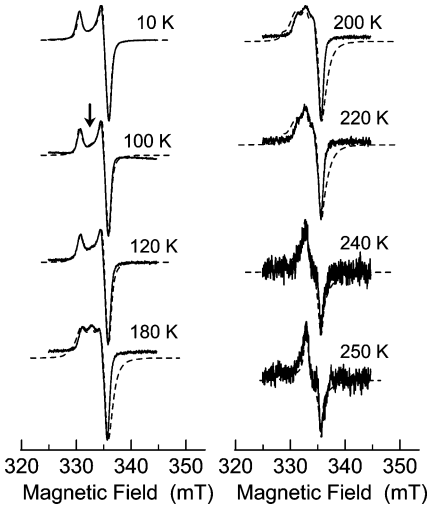


**Figure 5.** Temperature-dependent ESR spectra of NIPSOO tethered on the solid surface of PTFE in a vacuum. Observed spectra are shown with solid lines, and simulated spectra are shown with broken lines. Simulation spectra were calculated using the three *g* values (2.0355 ± 0.00005, 2.0080 ± 0.00005, 2.0023 ± 0.00005) and each correlation time at the corresponding temperature.

Temperature-dependent ESR spectra of NIPSOO observed in the temperature range from 10 to 250 K are shown in Figure 5 with solid lines. The spectrum observed at 10 K is a characteristic powder pattern of a rigid limit and is identical with that of the IPSOO at 10 K.[1] The simulated spectrum at 10 K using the three principal values of the **g**-tensor ($g_1 = 2.0355 \pm 0.00005$, $g_2 = 2.0080 \pm 0.00005$, and $g_3 = 2.0023 \pm 0.00005$) in a rigid limit is in good agreement with the observed spectrum (shown in Figure 5 at 10 K with the broken line). The three principal values of the **g**-tensor used in the simulation are the same as those of IPSOO. On the other hand, we reported that the *g* values of the peroxy radicals of PTFE were $g_1 = 2.0429$, $g_2 = 2.0081$ and, $g_3 = 2.0018$, and $g_{iso} = 2.0176$.[16] These values are not identical with those of $g_1 = 2.0355$, $g_2 = 2.0080$, $g_3 = 2.0023$ and $g_{iso} = 2.0153$ of the NIPSOO. Accordingly, these results strongly suggest that PS propagating radicals converted to PS peroxy radicals.

Although the shape of the spectrum of NIPSOO observed at 100 K is almost the same as that observed at 10 K, the depth of the valley between peaks (shown with an arrow) slightly decreases in relation to that observed at 10 K. The decrease suggests that a small-scale motion occurs at the temperature. The observed spectrum (shown in Figure 5 at 100 K with a solid line) fits well with the simulated one calculated using the same *g* values of the rigid limit and anisotropic correlation times, $\tau_1 = \tau_2 = (8.5 \pm 0.2) \times 10^{-8}$ s and $\tau_3 = (1.0 \pm 0.2) \times 10^{-7}$

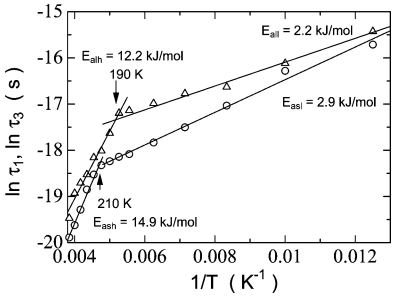


**Figure 6.** Arrhenius plot of correlation time $\tau$ of NIPSOO vs inverse temperature. ○, Short correlation time $\tau_1$; △, long correlation time $\tau_3$. $E_{all}$ and $E_{alh}$ are activation energies of a long correlation time in the temperature ranges from 100 to 190 K and from 190 to 250 K. $E_{asl}$ and $E_{ash}$ are activation energies of a short correlation time in the temperature ranges from 100 to 210 K and from 210 to 250 K.

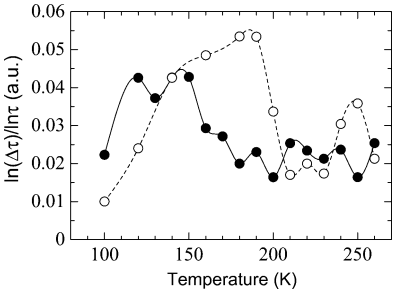


**Figure 7.** A relative anisotropy of correlation times, which is defined as $\ln(\Delta\tau)/\ln\tau_o$, is plotted against observation temperature. NIPSOO, ○ with the − − − line; IPSOO, ● with − line.

s. The anisotropic correlation time corresponds to the different residence time in each site and shows an anisotropic motional mode. All simulated spectra at the elevated temperatures were calculated using the same principal $g$ values except for each correlation time (shown in Figure 5 with broken lines). The spectral change of NIPSOO with increasing temperature is due to the molecular motion of NIPSOO with the corresponding correlation time. For example, the anisotropic correlation times at 190 K were calculated as $\tau_1 = \tau_2 = (1.3 \pm 0.1) \times 10^{-8}$ s corresponding to a short correlation time and $\tau_3 = (3.4 \pm 0.1) \times 10^{-8}$ s corresponding to a long correlation time. The anisotropic motion of NIPSOO corresponding to long and short correlation times decreased with increasing temperature (Figure 6).

Figure 6 shows Arrhenius plots of $\tau$ of NIPSOO versus inverse temperature. The long and short correlation times are shown with △ and ○, respectively. The long correlation time decreases with temperature increasing and steeply decreases above 190 K. The activation energy ($E_{all}$) of the motion was 2.2 ± 0.2 kJ/mol, which was derived from the slope of the line depicted by the least-squares method in the temperature range from 100 to 190 K. The short correlation time also decreases with temperature increasing and steeply decreases above 210 K. The activation energy ($E_{asl}$) of the motion in the temperature range from 100 to 210 K was calculated as 2.9 ± 0.2 kJ/mol. The values of $E_{all}$ and $E_{asl}$ are very small and almost identical. Thus, the corresponding motional mode of NIPSOO may be a small-scale motion with an anisotropic tumbling motion on the PTFE surface. When the observation temperature was above 190 K, the long correlation times steeply decrease with increasing temperature. The activation energy ($E_{alh}$) of the motion in the temperature range from 190 to 250 K was estimated as 12.2 ± 0.2 kJ/mol. For the short correlation time, the activation energy ($E_{ash}$) of the motion in the temperature range from 210 to 250 K was calculated as 14.9 ± 0.2 kJ/mol. The $E_{alh}$ and $E_{ash}$ are almost the same value. Since the difference between $\tau_3$ and $\tau_1$ values decreased above 190 K, the anisotropic motional mode changed into a slightly anisotropic one above 190 K (Figure 6). Both the small anisotropy between the short and long correlation times and the close activation energy suggest a similar motional mode above 190 K. The ESR line shape at 250 K with correlation time $\tau_1 = \tau_2 = (3.0 \pm 0.1) \times 10^{-9}$ s corresponding to a short correlation time and $\tau_3 = (6.0 \pm 0.1) \times 10^{-9}$ s corresponding to a long correlation time reveals that NIPSOO is in a free rotational mode having a slightly anisotropic motion. Thus, the NIPSOO probably untangled the pseudo entanglements, is protruded from the PTFE surface, and is at an almost free rotational state, which is defined as a tail state (illustrated in Figure 4). This indicates a motional transition from the train state to the tail state. The train−tail motional transition temperature is defined at 200 K due to the midpoint of the two alteration points of 190 and 210 K. The 20 K difference of the alteration points 190 and 210 K corresponding to long and short correlation times cannot be explained obviously. However, a motional mode with a long correlation time corresponding to a slow motion may be activated in a lower temperature range to achieve the train−tail transition.

The train−tail transition is not a conformation change in a small space but a transition with large space. On the other hand, a glass transition temperature reveals a relaxation due to a cooperative motion with a correlation length of chain segments in the bulk. It seems that the motion of the PS chains in the bulk at around the glass transition temperature may not correspond to the motion with a large space like the train−tail transition because the transition needs a large space for free rotation but it is hard to produce the space in the bulk at around the glass transition temperature.

Figure 7 shows a temperature dependence of a normalized anisotropy index of the correlation times defined as $\ln \Delta\tau/\ln \tau_o = (\ln \tau_3 - \ln \tau_1)/\ln((\tau_1 + \tau_2 + \tau_3)/3)$. The indexes of the IPSOO (shown with ●) and NIPSOO (shown with ○) showed the same tendency against an increment of temperature, the $\ln \Delta\tau/\ln \tau_o$ initially increased and reached relatively high values (more than 0.04) with an increase in temperature, but the value steeply decreased with a further increment of temperature. The steep drops were observed around 150 and 190 K for the IPSOO and NIPSOO, respectively. These temperatures correspond to the onset of the protruding of the PS chains from the PTFE surface. The high anisotropy of correlation times of the NIPSOO spreads over the temperature range from 140 to 190 K where that of the IPSOO is from 120 to 150 K. The anisotropic motion of NIPSOO with a wide temperature-range compared to that of IPSOO is probably due to interactions such as contact and pseudo entanglement between inter- and neighboring NIPSOO tethered on the solid surface of PTFE. We seem that the wide temperature range of the NIPSOO may be mainly due to pseudo entanglements.

## Conclusions

The molecular motion of NIPSOO tethered on the solid surface of PTFE in a vacuum was investigated in the temperature range from 10 to 250 K by ESR. The onset of an anisotropic tumbling motion of NIPSOO on the PTFE surface at a train state was 100 K. Above 200 K, the NIPSOO protruded from the PTFE surface and resulted in a free-rotational state with a slight anisotropy as a tail state. The activation energy of the molecular motion of NIPSOO at the tail state was calculated as 12.2−14.9 kJ/mol. The transition temperature and activation energy of NIPSOO were high compared to those of 160 K and 8.3−9.2 kJ/mol of the IPSOO tethered on the solid surface of

PTFE. The relative anisotropic motion of the NIPSOO exhibited a wide temperature range compared to that of IPSOO. The wide temperature range of motional anisotropy, high-transition temperature, and activation energy of the NIPSOO compared to those of the IPSOO are probably due to contact and pseudo entanglement between inter- and neighboring-NIPSOO chains on the PTFE surface.

## References and Notes


(1) Sakaguchi, M.; Yamamoto, K.; Miwa, Y.; Shimada, S.; Sakai, M.; Iwamura, T. *Macromolecules* **2007**, *40*, 1708.
(2) Mansfield, K. F.; Theodorou, N. *Macromolecules* **1991**, *24*, 6283.
(3) Forrest, J. A.; Dalnoki-Veress, K.; Stevens, J. R.; Dutcher, J. R. *Phys. Rev. Lett.* **1996**, *77*, 2002.
(4) Forrest, J. A.; Dalnoki-Veress, K.; Stevens, J. R.; Dutcher, J. R. *Phys. Rev. E* **1997**, *56*, 5705.
(5) Forrest, J. A.; Svanberg, C.; Revesz, K.; Rodahl, M.; Torell, L. M.; Kasemo, B. *Phys. Rev. E* **1998**, *58*, R1226.
(6) Ngai, K. L.; Rizos, A. K.; Plazek, D. J. *J. Non-Cryst. Solids* **1998**, *435*, 235−237.
(7) Doruker, P.; Mattice, W. L. *Macromolecules* **1999**, *32*, 194.
(8) Kajiyama, T.; Tanaka, K.; Takahara, A. *Macromolecules* **1997**, *30*, 280.
(9) Satomi, N.; Takahara, A.; Kajiyama, T. *Macromolecules* **1999**, *32*, 4474.
(10) Kawaguchi, D.; Tanaka, K.; Takahara, A.; Kajiyama, T. *Macromolecules* **2001**, *34*, 6164.
(11) Kawaguchi, D.; Tanaka, K.; Kajiyama, T.; Takahara, A.; Tasaki, S. *Macromolecules* **2003**, *36*, 1235.
(12) Tanaka, K.; Takahara, A.; Kajiyama, T. *Macromolecules* **2000**, *33*, 7588.
(13) Pratt, F. L.; Lancaster, T.; Brooks, M. L.; Blundell, S. J.; Prokscha, T.; Morenzori, E.; Suter, A.; Luetkens, H.; Khasanov, R.; Scheuermann, R.; Zimmermann, U.; Shinotsuka, K.; Assender H. E. *Phys. Rev. B* **2005**, *72*, 121401(R).
(14) Sakaguchi, M.; Yamaguchi, T.; Shimada, S.; Hori, Y. *Macromolecules* **1993**, *26*, 2612.
(15) Sakaguchi, M.; Shimada, S.; Hori, Y.; Suzuki, A.; Kawaizumi, F.; Sakai, M.; Bandow, S. *Macromolecules* **1995**, *28*, 8450.
(16) Shimada, S.; Suzuki, A.; Sakaguchi, M.; Hori, Y. *Macromolecules* **1996**, *29*, 973.
(17) Yamamoto, K.; Shimada, S.; Tsujita, Y.; Sakaguchi, M. *Polymer* **1997**, *38*, 6327.
(18) Sakaguchi, M.; Shimada, S.; Yamamoto, K.; Sakai, M. *Macromolecules* **1997**, *30*, 3620.
(19) Yamamoto, K.; Shimada, S.; Sakaguchi, M.; Tsujita, Y. *Macromolecules* **1997**, *30*, 6575.
(20) Sakaguchi, M.; Shimada, S.; Yamamoto, K.; Sakai, M. *Macromolecules* **1997**, *30*, 8521.
(21) Sakaguchi, M.; Yamamoto, K.; Shimada, S. *Macromolecules* **1998**, *31*, 7829.
(22) Yamamoto, K.; Suenaga, S.; Shimada, S.; Sakaguchi, M. *Polymer* **2000**, *41*, 6573.
(23) Sakaguchi, M.; Yamamoto, K.; Miwa, Y.; Hara, S.; Sugino, Y.; Okamoto, S.; Sakai, M.; Shimada, S. *Macromolecules* **2004**, *37*, 8128.
(24) Sakaguchi, M.; Sohma, J. *J. Polym. Sci., Polym. Phys. Ed.* **1975**, *13*, 1233.
(25) Heinzer, J. *Mol. Phys.* **1971**, *22*, 167.
(26) Iwasaki, M.; Sasaki, Y. *J. Polym. Sci., Part* A-2 **1968**, *6*, 1968.
(27) Kevan, L.; Schlick, S. *J. Phys. Chem.* **1986**, *90*, 1998.
(28) Kurokawa, N.; Sakaguchi, M.; Sohma, J. *Polym. J.* **1978**, *10*, 93.
(29) Sakaguchi, M.; Kashiwabara, H. *J. Polym. Sci., Polym. Lett. Ed.* **1980**, *18*, 563.
(30) Sakaguchi, M.; Sohma, J. *J. Appl. Polym. Sci.* **1978**, *22*, 2915.
(31) Sakaguchi, M.; Yamamoto, K.; Shimada, S.; Sakai, M. *J. Polym. Sci., Part B: Polym. Phys.* **1998**, *36*, 2095.
(32) Yamamoto, K.; Shimada, S.; Sakaguchi, M. *Polym. J.* **1997**, *29*, 370.
(33) *CRC Hand Book of Chemistry and Physics*, 76th ed.; Lide, D. R., Ed. CRC Press: Boca Raton, FL, 1995−1996; pp 9−31.
(34) Yoon, D. Y.; Sundararajan, P. R.; Flory, P. J. *Macromolecules* **1975**, *8*, 776.


MA701925V